

Special Collection

Interplay between Conductivity, Matrix Relaxations and Composition of Ca-Polyoxyethylene Polymer Electrolytes

Gioele Pagot,^{*[a]} Ketì Vezzù,^[a] Cynthia Susana Martinez-Cisneros,^[b] Claire Antonelli,^[c] Belen Levenfeld,^[b] Alejandro Varez,^[b] Jean-Yves Sanchez,^[b, d] and Vito Di Noto^{*[a, b]}

In this report, the conductivity mechanism of Ca²⁺-ion in polyoxyethylene (POE) solid polymer electrolytes (SPEs) for calcium secondary batteries is investigated by broadband electrical spectroscopy studies. SPEs are obtained by dissolving into the POE hosting matrix three different calcium salts: CaTf₂, Ca(TFSI)₂ and CaI₂. The investigation of the electric response of the synthesized SPEs reveals the presence in materials of two polarization phenomena and two dielectric relaxation events. It is demonstrated that the nature of the anion (*i.e.*, steric

hindrance, charge density and ability to act as coordination ligand) and the density of “dynamic crosslinks” of SPEs is fundamental in the establishment of ion-ion/ion-polymer interactions. The long-range charge migration processes occurring along the two revealed percolation pathways of the electrolytes are generally coupled with the polymer host dynamics and depend on the temperature and the anion nature. This study offers the needed tools for understanding Ca²⁺ conduction in POE-based electrolytes.

1. Introduction

In last decade, the world energy economy system is undergoing a radical metamorphosis. The policies pursued by both national governments of the major world economic powers, and by supranational institutions, are devoted towards the development of sustainable methods for energy conversion with a lower environmental impact with respect to the use of fossil fuels.^[1] Among these, renewable energy sources (*e.g.*, solar, wind, tides, *etc.*) are the most promising systems to be exploited.^[2] Nevertheless, they suffer from important disadvantages including the intermittent production of energy and the typical misalignment between availability and demand, which

must be addressed with appropriate storage systems.^[3] Energy storage and conversion devices are also increasingly required to support the growing electric vehicle market. In this field, secondary batteries, and in particular lithium-ion batteries (LIBs), are among the most efficient and compact systems for both applications.^[4] Despite their high performance, both in terms of energy density and coulombic efficiency, LIBs are still too far from the fulfil of market request, especially in the field of electric mobility, due to their high cost and very low safety. In this regard, novel battery chemistries, which replace lithium with other inexpensive and well-distributed metals in the earth's crust, must be developed. Several metals have been proposed as anode materials, such as sodium,^[5] potassium,^[6] magnesium,^[7] and aluminum.^[8] More recently, calcium has attracted the attention of scientists as an alternative to lithium in the development of secondary batteries.^[9] Despite a lower theoretical specific capacity with respect to lithium (*i.e.*, 3.86 and 1.34 Ahg⁻¹ for Li and Ca, respectively), calcium is 2'000 times more abundant than lithium in the Earth's crust, and it has a similar theoretical volumetric capacity and reduction potential (*i.e.*, 2.06 vs. 2.06 Ahcm⁻³ and -3.05 vs. -2.87 V against SHE for Li and Ca, respectively).^[9e] Thus, the development of secondary calcium batteries (CABs) would ensure the production of highly efficient and low cost energy storage devices, which could fill the gap in the demand requested by the market. The very poor literature on Ca²⁺ ion-conducting materials able to deposit and strip calcium metal demonstrates that among the functional components the electrolyte is the main roadblock towards the development of CABs.^[9a-d,10] What is even more unknown into this field is how Ca²⁺ ions are coordinated and exchanged between different domains in the electrolyte, and thus the conductivity mechanism. In this regard, broadband electrical spectroscopy (BES) is the most appropriate technique which can unveil the long-range charge migration processes and experimentally demonstrate the correlations existing between the dynamics of the hosting matrix and the


[a] Dr. G. Pagot, Dr. K. Vezzù, Prof. V. Di Noto
Section of Chemistry for Technologies (ChemTech), Department of Industrial Engineering
University of Padova


Via Marzolo 9, 35131 Padova, Italy
E-mail: gioele.pagot@unipd.it
vito.dinoto@unipd.it


[b] Dr. C. S. Martinez-Cisneros, Prof. B. Levenfeld, Prof. A. Varez, Prof. J.-Y. Sanchez, Prof. V. Di Noto
Materials Science and Engineering Department
University Carlos III of Madrid
Av. de la Universidad 30, 28911 Leganés, Madrid, Spain

[c] Dr. C. Antonelli
Institut Européen des membranes (IEM)
Université de Montpellier, ENSCM, CNRS
Place Eugène Bataillon, 34095 Montpellier, France

[d] Prof. J.-Y. Sanchez
University Grenoble Alpes, LEPMI
38000 Grenoble, France

 Supporting information for this article is available on the WWW under <https://doi.org/10.1002/celec.202100475>

 An invited contribution to a joint Special Collection in memory of Prof. Jean-Michel Savéant

 © 2021 The Authors. ChemElectroChem published by Wiley-VCH GmbH. This is an open access article under the terms of the Creative Commons Attribution Non-Commercial License, which permits use, distribution and reproduction in any medium, provided the original work is properly cited and is not used for commercial purposes.

conductivity of active mobile ions.^[11] In details, BES studies analyze the dependence of the electric properties of a material on the frequency and the temperature. In this way, polarization phenomena and dielectric relaxation events can be revealed, which are the result of charge accumulation phenomena and/or dipole moment fluctuation of host materials, and the corresponding activation energies of these events can be determined.

In this report, a detailed study of the conductivity mechanism of a family of innovative Ca^{2+} poly(oxyethylene) (POE)-based polymer electrolytes for calcium batteries is investigated by BES studies. In particular, the long-range Ca^{2+} charge migration processes occurring into the investigated system are detected, revealing how this mechanism is modulated by the temperature, type of calcium counter-ion (*i.e.*, iodide (I^-), trifluoromethane sulfonate (Tf^-), and bis(trifluoromethanesulfonyl)imide (TFSI^-)), and host medium relaxation phenomena. It is important to notice that the detailed understanding of the long-range charge migration process in proposed electrolytes is fundamental to trigger the development of improved electrolytes exhibiting superior performance, durability, and suitability for application in Ca batteries.

2. Results and Discussion

2.1. Polarization Phenomena and Dielectric Relaxations

A detailed analysis of the electric response of the [POE (CaX_2)_{0.033}] electrolytes, with X^- equal to I^- , Tf^- , or TFSI^- , is carried out by analyzing the profiles of the complex permittivity and conductivity spectra as a function of frequency and temperature. The real components of the complex permittivity ($\epsilon'(\omega)$) and complex conductivity ($\sigma'(\omega)$) for the three samples are shown in Figure 1.

The inspection of the $\epsilon'(\omega)$ profiles allows for the identification of the following events: (i) two polarizations in the low-frequency region ($10^0 < f < 10^3$ Hz), indicated as " σ_{EP} " and " σ_{IP} "; and (ii) two dielectric relaxations in the high-frequency region ($10^3 < f < 10^6$ Hz), labelled as " α_{slow} " and " α_{fast} ". These events are: (i) in accordance with other Li^+ POE-based electrolytes elsewhere reported,^[12] and (ii) studied vs. temperature and frequency by fitting simultaneously the spectra of the complex permittivity and conductivity with the following general Equation 1:^[11a]

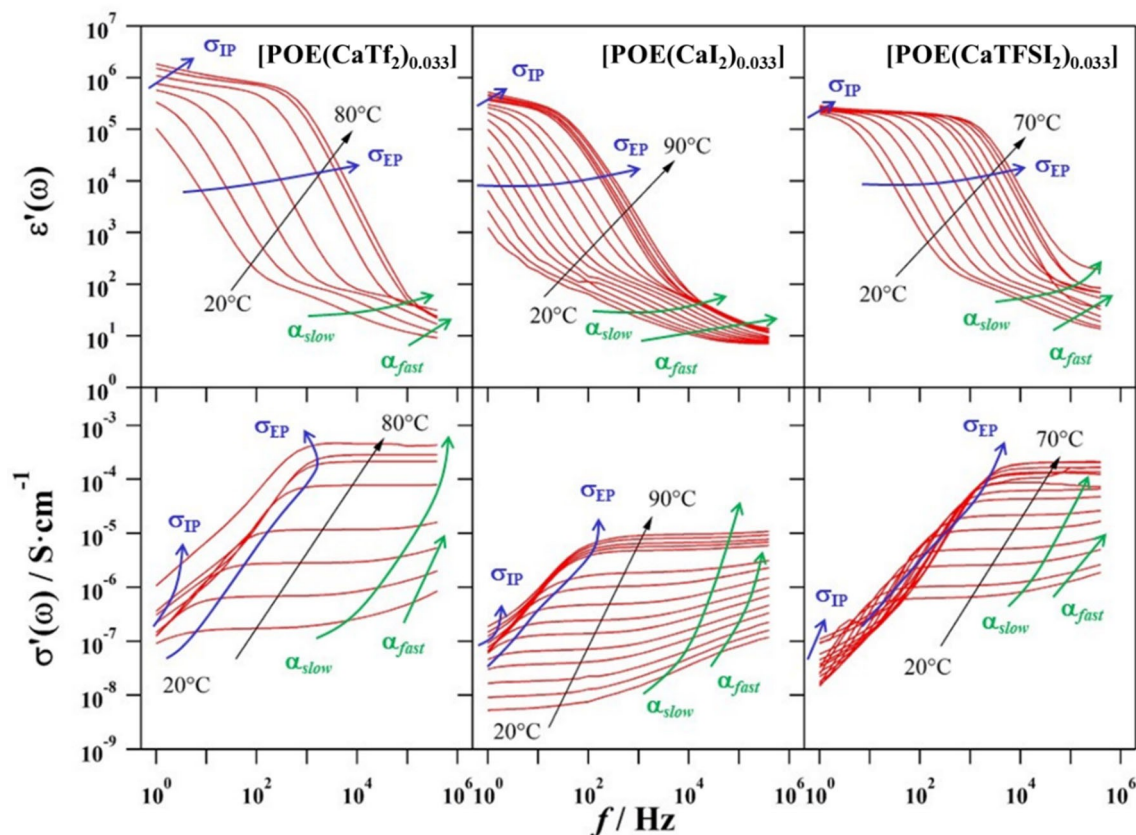


Figure 1. Real components of the complex permittivity ($\epsilon'(\omega)$, top three panels) and of the complex conductivity ($\sigma'(\omega)$, bottom three panels) vs. frequency for the three SPEs samples at different temperatures.

$$\varepsilon^*(\omega) = i \left(\frac{\sigma_0}{\varepsilon_0 \omega} \right)^N + \sum_{k=1}^2 \frac{\sigma_k (i\omega\tau_k)^{\gamma_k}}{i\omega [1 + (i\omega\tau_k)^{\gamma_k}]} + \sum_{j=1}^2 \frac{\Delta\varepsilon_j}{i\omega [1 + (i\omega\tau_j)^{\alpha_j}]^{\beta_j}} + \varepsilon_\infty \quad (1)$$

where $\varepsilon^*(\omega) = \varepsilon'(\omega) - i\varepsilon''(\omega)$ and $\sigma^*(\omega) = i\omega\varepsilon^*(\omega)$. The conductivity of the electrolyte at zero frequency gives rise to the first term of Equation 1, which is attributed to the residual conductivity of host matrix of the sample. The second term of Equation 1 refers to both the electrode polarization ($\sigma_{EP} \rightarrow k=1$) and to the interdomain polarization ($\sigma_{IP} \rightarrow k=2$). τ_k and σ_k are the relaxation times and the conductivity of the k^{th} polarization, while γ_k is an exponential factor ranging from 0.5 to 1. The third term corresponds to the Havriliak-Negami empirical equation,^[12a,13] that describes the two dielectric relaxations observed ($\alpha_{slow} \rightarrow j=1$ and $\alpha_{fast} \rightarrow j=2$). $\Delta\varepsilon_j$, τ_j , α_j and β_j correspond to the dielectric strength, relaxation time, symmetric and antisymmetric shape parameters of the j^{th} relaxation event, respectively. Finally, ε_∞ , which is the permittivity of the electrolyte at infinite frequency, accounts for the electronic contribution of bulk electrolytes. The imaginary components of the complex permittivity and complex conductivity, and $\tan \delta$, for the three samples, are shown in Figure S1, S2, and S3, respectively.

2.1.1. Polarization Phenomena

The polarization phenomena revealed in Figure 1 are attributed to: (i) the accumulation of charge between the sample and the blocking electrodes (σ_{EP}); and (ii) the formation of a conductivity pathway at the interfaces between nanodomains of the sample with a different permittivity (σ_{IP}). This latter finding indicates that the proposed [POE(CaX₂)_{0.033}] Ca-conducting electrolytes are heterogeneous at the mesoscale level (*i.e.*, amorphous and crystalline nanodomains). Additional information is retrieved from Figure 2, that reports on T^{-1} the fitting parameters of the electric response of the SPEs obtained by means of Equation 1. These parameters correspond to the conductivity values of the polarization events (σ_j), the frequencies (f_j) and the dielectric strength ($\Delta\varepsilon_j$) of the detected relaxation events.

The panels of Figure 2 show two temperature regions, I and II. In correspondence of T_m , a clear discontinuity is observed in the values of σ_{EP} (see the three top panels of Figure 2) at *ca.* 70 °C for [POE(CaI₂)_{0.033}] sample and *ca.* 60–65 °C for [POE(CaTf₂)_{0.033}] and [POE(CaTFSI₂)_{0.033}] electrolytes. T_m is in good agreement with the melting temperatures of the crystalline domains of the corresponding electrolytes reported in the literature.^[9e] The inspection of the top three panels of Figure 2 reveals that: (i) σ_{EP} is larger than σ_{IP} by *ca.* 2 orders of magnitude; and (ii) both σ_{EP} and σ_{IP} are present over the entire temperature range. These evidences demonstrate that, in

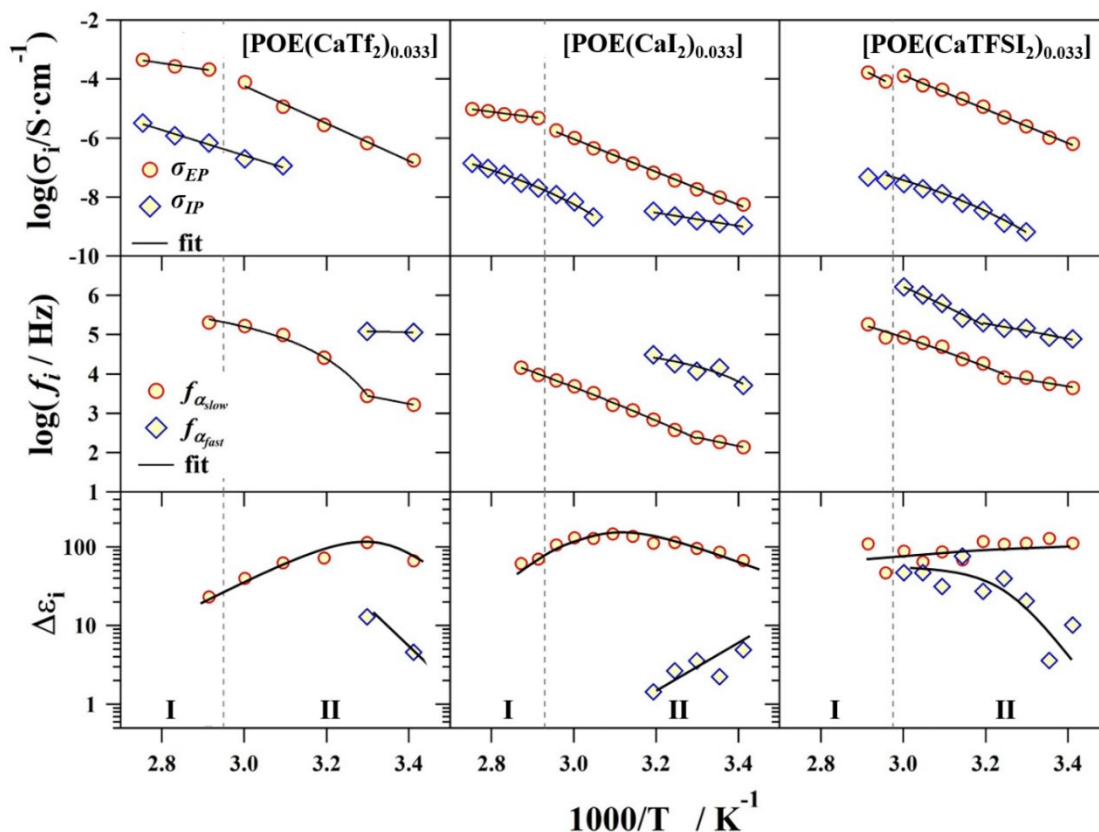


Figure 2. Dependence on T^{-1} of conductivity values associated to the polarization events (σ_j , top three panels); frequencies (f_j , middle three panels) and dielectric strength ($\Delta\varepsilon_j$, bottom three panels) of the two dielectric relaxation events " α_{slow} " and " α_{fast} " of the three [POE(CaX₂)_{0.033}] electrolyte samples. Regions I and II are delimited by the melting transition of materials (T_m , *ca.* 65 °C).^[9e]

accordance with Equation 2,^[14] the overall conductivity of a sample is the result of the superposition of conductivity values associated to the detected polarization phenomena:

$$\sigma_T = \sigma_0 + \sum_{k=1}^2 \sigma_k = \sigma_0 + \sigma_{EP} + \sigma_{IP} \quad (2)$$

A comparison of the value of each of the parameter of Equation 2 allows us to conclude that the largest contribution to the overall conductivity is provided by σ_{EP} . However, it is to be noticed that σ_{IP} , which is detected in both regions, I and II, does not reveal any discontinuity at T_m and presents values which increase in the order $[\text{POE}(\text{Ca}_2)_{0.033}] < [\text{POE}(\text{CaTFSI}_2)_{0.033}] < [\text{POE}(\text{CaTf}_2)_{0.033}]$ (see the top panels of Figure 2). This evidence clearly indicates that the mesoscale heterogeneities of SPEs play a crucial role in modulating the long-range charge migration processes of investigated electrolytes. In detail, at the interfaces between such heterogeneities likely associated to electrolyte nanodomains with a different permittivity (*i.e.*, amorphous and crystalline nanodomains), various types of charge accumulation are formed. Now, if we take into account that in the three different $[\text{POE}(\text{CaX}_2)_{0.033}]$ samples the host polymer matrix is kept constant, it is easy to admit that the detected differences in the relaxation modes are mainly associated to the type of anion adopted in the calcium salt. Indeed, it is observed that σ_{IP} decreases as the steric hindrance of the anion decreases. This evidence suggests that the Ca^{2+} ion is coordinated by both: (i) the oxygen atoms of the ligand functionalities belonging to the polymer backbone chain; and (ii) the anion Lewis bases of the Ca salts. In accordance with other studies,^[15] the interchain migration of Ca^{2+} ions plays a crucial role in modulating the long-range charge migration events in SPEs. This is described by σ_{IP} , which is attributed to the conductivity pathway associated to the exchange of cations between coordination sites present at the interfaces between polymeric domains with a different permittivity. At a given temperature, σ_{IP} values rise as the charge density of the anion increases in the order $\Gamma^- < \text{TFSI}^- < \text{Tf}^-$. This result witnesses that the steric hindrance of the anion inhibits the exchange of Ca^{2+} complexes between coordination sites present on different POE chains. In the medium-low temperature region ($20 \leq T \leq 60^\circ\text{C}$), this is further confirmed by the trends of σ_{EP} and σ_{IP} vs. temperature, which show: (i) an Arrhenius-like behavior for the $[\text{POE}(\text{Ca}_2)_{0.033}]$ and $[\text{POE}(\text{CaTf}_2)_{0.033}]$ SPEs: in this instances, hopping events, which are expected to be weakly coupled with the relaxations of the polymer host matrix, are crucial phenomena in the modulation of the overall conductivity mechanism of materials; and (ii) a VTF behavior for the $[\text{POE}(\text{CaTFSI}_2)_{0.033}]$ SPE, which demonstrates that in this sample the interchain hopping processes are significantly promoted by the segmental motions of the POE matrix that thus plays a crucial role in regulating the long-range charge migration processes in this system.

2.1.2. Dielectric Relaxation Events

For the proposed solid polymer electrolytes two dielectric relaxations are revealed in Region II, which are indicated as " α_{slow} " and " α_{fast} " (see the middle panels of Figure 2). Results show that at the same temperature the frequencies of α_{fast} are 1–2 order of magnitude higher than those of α_{slow} . For both α_{slow} and α_{fast} , $\log f$ vs T^{-1} exhibits a VTF behavior, suggesting that these two relaxations are associated to the "segmental mode" of polymer host matrix backbone chains. In accordance with other studies,^[11e,15] α_{fast} and α_{slow} are ascribed to the "segmental mode" corresponding to the diffusion of conformational states along the "free" and Ca-coordinated POE chains, respectively. The frequencies of both α_{slow} and α_{fast} increase progressively in the order $[\text{POE}(\text{Ca}_2)_{0.033}] < [\text{POE}(\text{CaTf}_2)_{0.033}] < [\text{POE}(\text{CaTFSI}_2)_{0.033}]$. This trend is ascribed to the type of interactions of the anions with the host polymer matrix, which increases as their steric hindrance is raised. In addition, as previously reported,^[9e] this trend is in agreement with the degree of crystallinity determined by means of DSC studies, which reveal a lower value for the TFSI⁻-based SPE and which provide critical information on ion-chain interactions.^[16] As a consequence, the "weak" interactions taking place through salt bridges between different POE chains (the "dynamic crosslinks")^[17] decrease in the strength on the type of anions, facilitating the interchain cation-exchange processes. In details, the decrease in the strength and density of "dynamic crosslinks" facilitates the α_{slow} and α_{fast} segmental motion phenomena, raising the frequencies of the corresponding dielectric relaxations. This interpretation is further supported by analyzing on T^{-1} the values of the dielectric strengths $\Delta\epsilon_i$ of α_{slow} and α_{fast} (see the bottom panels of Figure 2). Results show that the dielectric strength of α_{slow} : (i) is almost constant (*ca.* 100); and (ii) typically, is 1–2 orders of magnitude much larger than the dielectric strength of α_{fast} . This indicates that, in accordance with the Fröhlich and Kirkwood theory applied to polymers,^[18] among the detected dielectric relaxations, α_{slow} is expected to be the most intense owing to the stronger dipole moments of the polymer backbone chains. Actually, $\Delta\epsilon_{\alpha_{slow}}$ depends on: (i) the square of the overall dipole moment of the POE chains coordinating the Ca^{2+} complexes *per* volume unit; and (ii) the strength of the interactions existing between the chain and the environment, which acts to decrease the values of $\Delta\epsilon$ as the density of the interactions increases. It is observed that at 50°C the density of weak "dynamic crosslinks" decreases in the order $\text{Tf}^- \gg \text{TFSI}^- > \Gamma^-$, thus witnessing that the chains complexing Ca^{2+} are less involved in interactions with the environment for Γ^- anion. Accordingly, the conductivity of $[\text{POE}(\text{CaTf}_2)_{0.033}]$ SPE is the highest, thus confirming that the mobility of Ca^{2+} in this electrolyte is larger, likely owing to a better coupling of hopping processes and segmental motion relaxations of polymer chains. On the other hand, the dielectric strength of α_{fast} increases by more than one order of magnitude in this direction: $[\text{POE}(\text{Ca}_2)_{0.033}] < [\text{POE}(\text{CaTf}_2)_{0.033}] < [\text{POE}(\text{CaTFSI}_2)_{0.033}]$ (see the bottom panels of Figure 2). Results indicate that the anion influences also the α_{fast} mode. Indeed, both Tf^- and TFSI^- anions, which are expected to complete the octahedral

coordination of Ca^{2+} metal bridges between POE chains,^[19] act to reduce the strength of the interchain interactions between free POE chains, reducing the size of these salt “free” nanodomains of the electrolytes. In details, results show that: (i) in $\Delta\epsilon_{\alpha_{fast}}$ the density and strength of the interactions of POE “free chains” with the environment rise in the order $\text{TFSI}^- < \text{Tf}^- < \text{I}^-$; while (ii) for $[\text{POE}(\text{CaTFSI}_2)_{0.033}]$ SPE, $\Delta\epsilon_{\alpha_{slow}} \approx \Delta\epsilon_{\alpha_{fast}}$ thus suggesting that TFSI^- is the best anion. However, it is observed that creeping starts earlier for TFSI^- (ca. 70 °C), later for Tf^- (ca. 85 °C), and was not observed for I^- -based SPE. Moreover, a higher cation transference number is typically reported in the literature for Tf^- -based SPEs with respect to TFSI^- .^[20] Thus, $[\text{POE}(\text{CaTf}_2)_{0.033}]$ SPE could result in a higher cationic conductivity, and deserves to be considered as the best choice in these systems. Nevertheless, the studies here reported clearly demonstrate that the TFSI^- anion improves the delocalization of Ca^{2+} complexes in materials by increasing the density of weak “dynamic crosslinks” between different POE chains. Concurrently, this situation results also in a higher delocalization of the negative charge, as proven by early studies in the literature.^[21] This is consistent with the increase in the intensity of α_{fast} mode, which is triggered by the more facile fluctuations of the dipole moments localized along the POE macromolecules of host polymer matrix. Higher molecular weight POEs are not expected to affect the polarization phenomena of the hosting matrix, since the proposed material is already above the entanglement weight (i.e., ca. 3'000 g mol^{-1}).^[22] Nevertheless, other properties of the SPE could be modulated, such as its elasticity or adhesive behavior.^[23]

2.2. Activation Energies

The activation energy (E_a) associated to both σ_{EP} and σ_{IP} are evaluated by fitting the σ_i profiles shown in the top three panels of Figure 2 with an Arrhenius or VTF equation. Similarly, the activation energies of both α_{slow} and α_{fast} are determined by fitting the profiles shown in the middle panels of Figure 2 by Arrhenius- or Vogel Tamman Fulcher Hesse-like (VTFH) equations. Results are summarized in Figure 3.

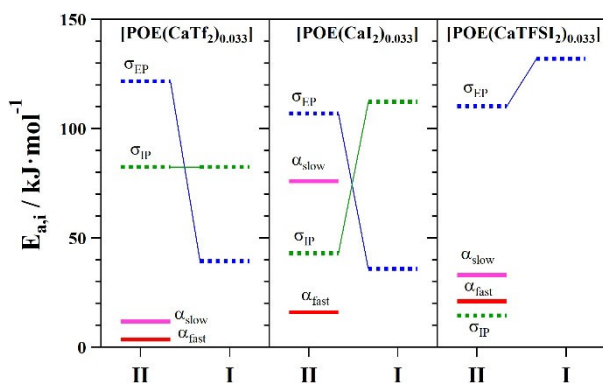


Figure 3. Activation energies ($E_{a,i}$) for each polarization phenomenon and relaxation of the proposed polymer electrolytes. I and II indicate respectively the high ($T > T_m$) and low ($T < T_m$) temperature regions.

For $[\text{POE}(\text{CaI}_2)_{0.033}]$, the activation energies of σ_{EP} and σ_{IP} differ from those of α_{slow} and α_{fast} . This suggests that in I^- -based electrolyte both σ_{EP} and σ_{IP} are less correlated to the segmental motions of POE. In $[\text{POE}(\text{CaTFSI}_2)_{0.033}]$, σ_{EP} is also less correlated to the α relaxations of the POE host matrix, while σ_{IP} is significantly triggered by both α_{fast} and α_{slow} modes. Indeed, in Region II of $[\text{POE}(\text{CaTFSI}_2)_{0.033}]$ the activation energy of σ_{IP} corresponds with that characterizing α_{fast} and α_{slow} (i.e., $15 < E_a < 35 \text{ kJ mol}^{-1}$). This confirms that in $[\text{POE}(\text{CaTFSI}_2)_{0.033}]$ the long-range charge migration phenomena at the interface between different nanodomains of the SPE is modulated by the segmental modes of the polymer host matrix. In accordance with other papers,^[13] the rate-determining step in the long-range charge migration process is the exchange of ions between delocalization bodies (DBs). In the present case, a DB consists in a volume of amorphous $[\text{POE}(\text{CaTFSI}_2)_{0.033}]$ electrolyte within which the ions are exchanged between coordination sites at a much faster rate with respect to the average migration time associated with the overall conductivity. In these conditions, in the time scale of the overall conductivity, the ions can be considered delocalized within each DB. The exchange of ions between different DBs is completely correlated to the α_{slow} and α_{fast} segmental mode dynamics. The $[\text{POE}(\text{CaTf}_2)_{0.033}]$ SPE exhibits the same behavior in E_a as that of $[\text{POE}(\text{CaI}_2)_{0.033}]$. In this case, both in Region I and in Region II a weak correlation is observed between σ_{EP} and σ_{IP} conductivity pathways and the segmental mode relaxations of the POE host matrix (α_{fast} and α_{slow}). Taking all together, results witness that, in the electrolytes here proposed, the hopping processes of Ca^{2+} species at the interfaces between domains with a different permittivity are mediated by: (i) the segmental mode of both α_{fast} and α_{slow} relaxations; (ii) the weak “dynamic crosslinks” involving Ca^{2+} complexes; (iii) the exchange of anion ligands; and (iv) the reorientation of relaxation processes of local dipoles similarly to that previously described for POE- MgX_2 electrolytes ($\text{X}=\text{Cl}, \text{I}$).^[11e,24] In summary, the nature of the anion is of crucial importance in modulating the two types of conductivity pathways contributing to the overall conductivity of the $[\text{POE}(\text{CaX}_2)_{0.033}]$ SPEs.

2.3. Diffusion Coefficients and Average Charge Migration Distances

Further insights on the role played by the anions and the dynamics of host polymer matrix in the conduction mechanism of materials can be achieved by correlating the diffusion coefficient associated to each conductivity pathway to the frequencies of the α_{slow} and α_{fast} dielectric relaxations. The diffusion coefficient, D_{oi} , associated to the conductivity σ_i is determined using Equation 3:^[15]

$$D_{oi} = \frac{RT\sigma_i}{Z^2 C_i F^2} \quad (3)$$

where R is the gas constant, T is the absolute temperature, σ_i is the conductivity of the i -th polarization event, Z is the charge of

the mobile species (in this case, it is assumed that the mobile charged species is Ca^{2+} , i.e., $Z=2$), F is the Faraday constant and C is the concentration of doping salt. Figure 4 plots the diffusion coefficients of both σ_{EP} ($D_{\sigma_{EP}}$, top panels) and σ_{IP} ($D_{\sigma_{IP}}$, bottom panels) vs. the frequency of both α_{slow} and α_{fast} .

Interestingly, a very good linear correlation exists between $\log(D_{\sigma_{EP}})$ and both $\log(f_{\alpha_{slow}})$ and $\log(f_{\alpha_{fast}})$ for all the three proposed electrolytes. Results clearly reveal that both α_{slow} and α_{fast} are influencing significantly the conductivity associated to the electrode polarization event of these electrolytes. This confirms that in the σ_{EP} pathway the mechanism modulating the long-range charge migration, which takes place owing to the charge exchange processes between DBs, is significantly correlated to both the α_{slow} and α_{fast} segmental modes of POE chains. Here, DBs are likely consistent with the amorphous domains of POE- CaX_2 electrolytes. On the other hand, the correlation between $\log(D_{\sigma_{IP}})$ and both $\log(f_{\alpha_{slow}})$ and $\log(f_{\alpha_{fast}})$ is significantly dependent on the type of anion present in the POE- CaX_2 electrolytes. These evidences confirm that, similarly to the electrolytes based on other divalent M^{2+} ions, the anion plays a crucial role in local hopping processes of ion species between coordination sites present at the interfaces between domains with a different permittivity.^[11e,24] In this case, in accordance with other studies,^[15,25] α_{slow} and α_{fast} are fundamental in facilitating interchain hopping processes of ion complexes between oxygenated coordination sites present in different neighboring POE chains.

The diffusion coefficients above described can be used to determine the dependence on temperature of the average charge migration distance $\langle r_i \rangle$ of both electrode polarization (σ_{EP}) and interdomain polarization (σ_{IP}) conductivity pathways. $\langle r_i \rangle$ is obtained by means of the Einstein-Smoluchowski equation (Equation 4):^[26]

$$\langle r_i \rangle = \sqrt{6D_{\sigma_i}\tau_i} \quad (4)$$

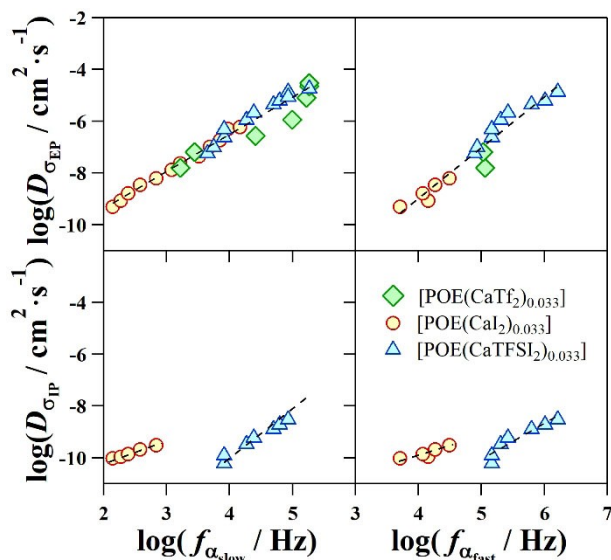


Figure 4. Diffusion coefficients (D_{σ_i}), evaluated from σ_i data by means of Equation 3, as a function of the frequencies of α_{slow} and α_{fast} .

where D_{σ_i} is the diffusion coefficient associated to the conductivity σ_i and τ_i is the relaxation time of the σ_{EP} and σ_{IP} polarization events obtained by fitting the real and imaginary components of $\epsilon^*(\omega)$ profiles by means of Equation 1. The dependence on temperature of the average charge migration distance $\langle r_i \rangle$ for both σ_{EP} and σ_{IP} is shown in Figure 5.

$\langle r_{EP} \rangle$ is on the order of 20–110 nm, while $\langle r_{IP} \rangle$ presents values which, with respect to $\langle r_{EP} \rangle$, are lower than 2 orders of magnitude. This confirms that $\langle r_{EP} \rangle$ corresponds to the long-range charge migration pathway, which involves the exchange processes of ion species between DBs with a size of the order of 20–110 nm. $\langle r_{IP} \rangle$, which is on the order of ca. 1 nm or less, is attributed to the local exchange of Ca^{2+} species between coordination sites located at the interfaces between neighboring nanodomains of the electrolyte with different permittivity. $\langle r_{EP} \rangle$ increases as T is raised, suggesting that the charge migration process between DBs is a thermally-activated event. Finally, it is observed that, for a given temperature, $\langle r_{EP} \rangle$ increases in the order $[\text{POE}(\text{CaI}_2)_{0.033}] < [\text{POE}(\text{CaTf}_2)_{0.033}] < [\text{POE}(\text{CaTFSI}_2)_{0.033}]$. This latter outcome demonstrates that the anion plays a crucial role in the modulation of electrolyte mesoscale morphologies owing to its interaction with the cation and the matrix. Indeed, higher is its involvement in dynamic crosslinks, larger is the size of the amorphous domains which correspond to the DBs that are responsible of the long-range charge migration mechanism.

3. Conclusion

This study sheds light on the conduction mechanisms occurring in $[\text{POE}(\text{CaX}_2)_{0.033}]$ SPEs. These electrolytes, which differ only for the anion of the calcium salt, present a different conductivity. The long-range Ca^{2+} charge migration mechanism is mediated by the exchange of Ca-based coordination species between different POE chains. This phenomenon is modulated by the type of anions of the CaX_2 salts and by the segmental modes of POE host polymer, which play a crucial role in the conduction mechanisms of the three proposed $[\text{POE}(\text{CaX}_2)_{0.033}]$ SPEs. It is revealed that in proposed materials two conductivity pathways

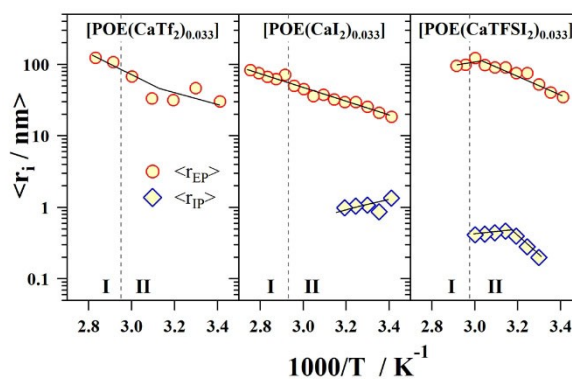


Figure 5. Dependence of average charge migration distance $\langle r_i \rangle$ on temperature. $\langle r_{EP} \rangle$ and $\langle r_{IP} \rangle$ are associated to the electrode polarization (σ_{EP}) and the interdomain polarization (σ_{IP}), respectively.

(i.e., σ_{EP} and σ_{IP}) are contributing to the overall conductivity (σ_T) of proposed electrolytes. σ_{EP} and σ_{IP} are associated to the migration of ion species between “delocalization bodies” (DBs) or at the interfaces between different nanodomains of SPEs, respectively. It is disclosed that: (i) segmental motions, (α_{slow} and α_{fast}) of host polymer nanodomains both modulate the σ_{EP} and σ_{IP} conductivity pathways; (ii) σ_T in [POE(CaX₂)_{0.033}] SPEs, which is the superposition of both σ_{EP} and σ_{IP} ($\sigma_T = \sigma_{EP} + \sigma_{IP}$), mostly corresponds to σ_{EP} ($\sigma_T \simeq \sigma_{EP}$). In particular, TFSI⁻, which is likely more delocalized than the other anions, enhances the density and reduces the strength of the weak “dynamic crosslinks” between POE chains that promote the interchain migration of Ca²⁺ ions. In this scenario, the exchange of Ca²⁺ ions between different coordination sites is facilitated. Indeed, DBs with larger sizes are thus formed, which correspond to amorphous domains of the [POE(CaTFSI₂)_{0.033}] and where the exchange of Ca²⁺ ions is so fast that the charge can be considered delocalized. In this condition, the long-range charge migration in σ_{EP} is only bottlenecked by the exchange of Ca²⁺ ions between different DBs. These migration events are completely coupled with the segmental mode dynamics of POE host chains. In the case of [POE(CaTf₂)_{0.033}], the overall conductivity mechanism is quite similar to that described above for [POE(CaTFSI₂)_{0.033}]. However, the Tf⁻ anions are likely less effective than TFSI⁻ at forming dynamic crosslinks between the macromolecular chains of the POE host due to their smaller steric hindrance and lower prevalence of -CF₃ groups. This somehow decreases the density and strength of the weak “dynamic crosslinks” that are crucial in the interchain hopping of Ca²⁺ ions. Finally, for [POE(CaI₂)_{0.033}], the I⁻ ions: (i) coordinate Ca²⁺ together with the oxygen atoms present along the same POE chain, similarly to what is revealed for other divalent cations such as Mg²⁺,^[11e] and (ii) are not very bulky, thus reducing significantly the density of crosslinks between different POE chains. These phenomena inhibit the interchain hopping of Ca²⁺, reducing the conductivity of [POE(CaI₂)_{0.033}] which, among the three proposed electrolytes, is the lowest. Taking all together, this study allows us to shed light on the effect of different anions on the conductivity mechanism of Ca-based solid polymer electrolytes, thus paving the way for the future development of calcium electrolytes for secondary batteries.

Experimental Section

Materials

POE (average MW 3 · 10⁵ g mol⁻¹), calcium iodide (CaI₂), calcium trifluoromethane sulfonate (CaTf₂), and calcium bis(trifluoromethanesulfonyl)imide, Ca(TFSI)₂ salts were supplied by Sigma-Aldrich.

Preparation of Polymer Electrolytes

The polymer electrolyte membranes containing different calcium salts are obtained in accordance with a previous procedure developed in our lab.^[9e,27] In details, three different water solutions

of PEO and the selected CaX₂ calcium salt (with X equal to I⁻, Tf⁻, or TFSI⁻) are prepared dissolving the proper amounts of the two components. A Ca:EO molar ratio of 0.033:1 is obtained, which corresponds to a EO:Ca molar ratio of 30:1. This molar ratio is properly selected in order to achieve the highest Ca²⁺ ionic conductivity.^[9e] The prepared solutions are stirred for 5 h and then freeze-dried at -20 °C for 48 h using a FreeZone instrument (LABCONCO, USA). Three different calcium solid polymer electrolyte (SPE) powders with a formula [POE(CaX₂)_{0.033}] are obtained. The polymer electrolytes in the form of membranes are prepared following a two-step procedure: (i) heating of the powders at 100 °C for 20 minutes onto a stainless-steel plate; and (ii) hot-pressing of the melted SPE at 50 kN maintaining the temperature of 100 °C. The three SPE membranes show a thickness in the range of 100–150 μm. The complete elimination of water traces from the SPEs is achieved heating the samples at 50 °C in vacuum for 12 h and storing them inside an Ar-filled glove box (H₂O < 1 ppm and O₂ < 1 ppm).

Broadband Electrical Spectroscopy Studies

Electrical spectroscopy studies are performed with an Impedance/Gain-Phase Analyzer SI1260 (Solartron, UK). Data are collected every 10 °C in the temperature range between 20 and 90 °C, with an accuracy greater than ±0.2 °C, and applying an alternating electric field of 0.1 V in the frequency range from 1 Hz to 10 MHz. Samples sandwiched between two stainless steel blocking electrodes of 11 mm of diameter are inserted into a sealed Nylon cell inside a glove box. The sealed cell thus obtained is used to measure Z' and Z'' on frequency and temperature. Complex conductivity (σ^*) and permittivity (ϵ^*) spectra are obtained using the following equations (Equation 5–6):^[11a]

$$\sigma^*(\omega) = \frac{1}{KZ^*(\omega)} \quad (5)$$

$$\sigma^*(\omega) = i\omega\epsilon_0\epsilon^*(\omega) \quad (6)$$

where ω is the angular frequency, Z* is the complex impedance, and K corresponds to the geometric cell constant in cm ($K = A/d$; A is the area of the electrode and d is the spacing). i is the imaginary unit and ϵ_0 refers to the vacuum permittivity.

Credit author statement

G. Pagot: Formal analysis, Writing - Original Draft; C.S. Martinez-Cisneros: Investigation, Supervision; C. Antonelli: Formal analysis; B. Levenfeld: Resources; A. Varez: Resources; K. Vezzù: Formal analysis, Writing - Original Draft; J-Y. Sanchez: Conceptualization, Supervision, Funding acquisition V. Di Noto: Formal analysis, Writing - Original Draft, Supervision, Funding acquisition.

Acknowledgements

This work has been supported by the European Union's Horizon 2020 research and innovation programme under grant agreement No 829145 (FETOPEN-VIDICAT). V. Di Noto thanks the University Carlos III of Madrid for the “Catedras de Excelencia UC3 M-Santander” (Chair of Excellence UC3 M-Santander).

Conflict of Interest

The authors declare no conflict of interest.

Keywords: conducting materials · broadband electrical spectroscopy · calcium electrolytes · solid polymer electrolytes · energy conversion

- [1] a) V. Di Noto, S. Lavina, G. A. Giffin, E. Negro, B. Scrosati, *Electrochim. Acta* **2011**, *57*, 4–13; b) M. Sawicki, L. L. Shaw, *RSC Adv.* **2015**, *5*, 53129–53154.
- [2] H. Mikulčić, J. Baleta, J. J. Klemesš, X. Wang, *J. Cleaner Prod.* **2021**, *292*.
- [3] M. Rezkallah, S. Singh, A. Chandra, B. Singh, H. Ibrahim, *Energies* **2020**, *13*.
- [4] a) B. Dunn, H. Kamath, J. M. Tarascon, *Science* **2011**, *334*, 928–935; b) G. Pagot, M. Bandiera, K. Vezzù, A. Migliori, R. Bertoncello, E. Negro, V. Morandi, V. Di Noto, *J. Mater. Chem. A* **2020**, *8*, 25727–25738.
- [5] a) W.-Q. Rong, J.-H. You, X.-M. Zheng, G.-P. Tu, S. Tao, P.-Y. Zhang, Y.-X. Wang, J.-T. Li, *ChemElectroChem* **2019**, *6*, 5420–5427; b) X.-M. Zhao, Y.-W. Yan, X.-X. Ren, L. Chen, S.-D. Xu, S.-B. Liu, X.-M. Wang, D. Zhang, *ChemElectroChem* **2019**, *6*, 1229–1234; c) W. Deng, X. Feng, Y. Xiao, C. Li, *ChemElectroChem* **2018**, *5*, 1032–1036; d) M. J. Aragón, P. Lavela, G. F. Ortiz, R. Alcántara, J. L. Tirado, *ChemElectroChem* **2018**, *5*, 367–374; e) N. Sabi, A. Sarapulova, S. Indris, S. Dsoke, V. Trouillet, L. Mereacre, H. Ehrenberg, I. Saadoune, *J. Power Sources* **2021**, *481*; f) T. Y. Yu, J. Y. Hwang, I. T. Bae, H. G. Jung, Y. K. Sun, *J. Power Sources* **2019**, *422*, 1–8.
- [6] a) Z. Wu, J. Zou, S. Chen, X. Niu, J. Liu, L. Wang, *J. Power Sources* **2021**, *484*; b) J. Touja, V. Gabaudan, F. Farina, S. Cavaliere, L. Caracciolo, L. Madec, H. Martinez, A. Boulaoued, J. Wallenstein, P. Johansson, L. Stievano, L. Monconduit, *Electrochim. Acta* **2020**, *362*; c) M. Arnaiz, A. Bothe, S. Dsoke, A. Balducci, J. Ajuria, *J. Electrochem. Soc.* **2019**, *166*, A3504–A3510; d) M. G. T. Nathan, W. B. Park, N. Naveen, S. Park, K. S. Sohn, M. Pyo, *J. Electrochem. Soc.* **2020**, *167*; e) V. Lakshmi, A. A. Mikhaylov, A. G. Medvedev, C. Zhang, T. Ramireddy, M. M. Rahman, P. Cizek, D. Golberg, Y. Chen, O. Lev, P. V. Prikhodchenko, A. M. Glushenkov, *J. Mater. Chem. A* **2020**, *8*, 11424–11434; f) C. Li, A. T. Bi, H. L. Chen, Y. R. Pei, M. Zhao, C. C. Yang, Q. Jiang, *J. Mater. Chem. A* **2021**, *9*, 5740–5750; g) E. J. Canto-Aguilar, M. A. Oliver-Tolentino, G. Ramos-Sánchez, I. González, *Electrochim. Acta* **2021**, *371*; h) J. Zou, S. Chen, Z. Wu, J. Gao, P. Chen, Q. Ran, S. Li, L. Wang, X. Niu, *J. Power Sources* **2020**, *480*.
- [7] a) F. Bertasi, C. Hettige, F. Sepehr, X. Bogle, G. Pagot, K. Vezzù, E. Negro, S. J. Paddison, S. G. Greenbaum, M. Vittadello, V. Di Noto, *ChemSusChem* **2015**, *8*, 3069–3076; b) F. Bertasi, F. Sepehr, G. Pagot, S. J. Paddison, V. Di Noto, *Adv. Funct. Mater.* **2016**, *26*, 4860–4865; c) V. Di Noto, S. Lavina, D. Longo, M. Vidali, *Electrochim. Acta* **1998**, *43*, 1225–1237; d) R. Dominko, J. Bitenc, R. Berthelot, M. Gauthier, G. Pagot, V. Di Noto, *J. Power Sources* **2020**, *478*, 229027; e) G. Pagot, K. Vezzù, A. Nale, M. Fauri, A. Migliori, V. Morandi, E. Negro, V. Di Noto, *J. Electrochem. Soc.* **2020**, *167*; f) N. Ishida, N. Yamazaki, T. Mandai, N. Kitamura, Y. Idemoto, *J. Electrochem. Soc.* **2020**, *167*; g) D. Hambali, Z. Osman, L. Othman, K. B. M. Isa, N. Harudin, *J. Polym. Res.* **2020**, *27*; h) K. Sone, Y. Hayashi, T. Mandai, S. Yagi, Y. Oaki, H. Imai, *J. Mater. Chem. A* **2021**, *9*, 6851–6860.
- [8] a) G. Pagot, K. Vezzù, S. G. Greenbaum, V. Di Noto, *J. Power Sources* **2021**, *493*, 229681; b) B. Zhang, Y. Zhang, J. Li, J. Liu, X. Huo, F. Kang, *J. Mater. Chem. A* **2020**, *8*, 5535–5545; c) Y. Liao, D. Wang, X. Li, S. Tian, H. Hu, D. Kong, T. Cai, P. Dai, H. Ren, H. Hu, Y. Li, Q. Xue, Z. Yan, X. Gao, W. Xing, *J. Power Sources* **2020**, *477*; d) M. Han, Z. Lv, L. Hou, S. Zhou, H. Cao, H. Chen, Y. Zhou, C. Meng, H. Du, M. Cai, Y. Bian, M. C. Lin, *J. Power Sources* **2020**, *451*; e) J. Li, W. Liu, Z. Yu, J. Deng, S. Zhong, Q. Xiao, F. chen, D. Yan, *Electrochim. Acta* **2021**, *370*; f) Q. Zhao, J. Zheng, Y. Deng, L. Archer, *J. Mater. Chem. A* **2020**, *8*, 23231–23238; g) T. Schoetz, O. Leung, C. P. De Leon, C. Zaleski, I. Efimov, *J. Electrochem. Soc.* **2020**, *167*; h) Q. Zhou, D. Wang, Y. Lian, S. Hou, C. Ban, Z. Wang, J. Zhao, H. Zhang, *Electrochim. Acta* **2020**, *354*; i) W. Guan, L. Wang, J. Tu, S. Jiao, *J. Electrochem. Soc.* **2020**, *167*.
- [9] a) J. Muldoon, C. B. Bucur, T. Gregory, *Chem. Rev.* **2014**, *114*, 11683–11720; b) E. Peled, *J. Electrochem. Soc.* **1979**, *126*, 2047–2051; c) D. Wang, X. Gao, Y. Chen, L. Jin, C. Kuss, P. G. Bruce, *Nat. Mater.* **2018**, *17*, 16–20; d) M. E. Arroyo-de Dompablo, A. Ponrouch, P. Johansson, M. R. Palacín, *Chem. Rev.* **2020**, *120*, 6331–6357; e) C. S. Martinez-Cisneros, A. Fernandez, C. Antonelli, B. Levenfeld, A. Varez, K. Vezzù, V. Di Noto, J. Y. Sanchez, *Electrochim. Acta* **2020**, *353*, 136525.
- [10] a) F. S. Genier, C. V. Burdin, S. Biria, I. D. Hosein, *J. Power Sources* **2019**, *414*, 302–307; b) D. Vanitha, S. A. Bahadur, N. Nallamuthu, A. Shunmuganarayanan, A. Manikandan, *J. Nanosci. Nanotechnol.* **2018**, *18*, 1723–1729.
- [11] a) V. Di Noto, G. A. Giffin, K. Vezzù, M. Piga, S. Lavina, in *Solid State Proton Conductors: Properties and Applications in Fuel Cells*, John Wiley & Sons, Chichester, U. K., **2012**, pp. 109–183; b) V. Di Noto, V. Münchow, M. Vittadello, J. C. Collet, S. Lavina, *Solid State Ionics* **2002**, *147*, 397–402; c) V. Di Noto, *J. Mater. Res.* **1997**, *12*, 3393–3403; d) V. Di Noto, M. Vittadello, S. G. Greenbaum, S. Suarez, K. Kano, T. Furukawa, *J. Phys. Chem. B* **2004**, *108*, 18832–18844; e) V. Di Noto, M. Vittadello, *Solid State Ionics* **2002**, *147*, 309–316.
- [12] a) S. Kitajima, F. Bertasi, K. Vezzù, E. Negro, Y. Tominaga, V. Di Noto, *Phys. Chem. Chem. Phys.* **2013**, *15*, 16626–16633; b) K. Vezzù, V. Zago, M. Vittadello, A. Bertuccio, V. D. Noto, *Electrochim. Acta* **2006**, *51*, 1592–1601.
- [13] V. Di Noto, G. Giffin, K. Vezzù, G. Nawn, F. Bertasi, T. H. Tsai, A. M. Maes, S. Seifert, B. E. Coughlin, A. M. Herring, *Phys. Chem. Chem. Phys.* **2015**, *17*, 31125–31139.
- [14] F. Bertasi, K. Vezzù, G. A. Giffin, T. Nosach, P. Sideris, S. Greenbaum, M. Vittadello, V. Di Noto, *Int. J. Hydrogen Energy* **2014**, *39*, 2884–2895.
- [15] V. Di Noto, M. Vittadello, K. Yoshida, S. Lavina, E. Negro, T. Furukawa, *Electrochim. Acta* **2011**, *57*, 192–200.
- [16] Y. Wang, W.-H. Zhong, T. Schiuff, A. Eyler, B. Li, *Adv. Energy Mater.* **2015**, *5*, 1400463.
- [17] V. Di Noto, M. Vittadello, *Solid State Ionics* **2002**, *147*, 309–316.
- [18] C. J. F. Böttcher, P. Bordewijk, *Dielectrics in Time-Dependent Fields*, Vol. 2, 2nd ed., Elsevier, Amsterdam, **1978**.
- [19] F. A. Cotton, G. Wilkinson, C. A. Murillo, M. Bochmann, *Advanced Inorganic Chemistry*, John Wiley and Sons, New York, **1999**.
- [20] a) F. Alloin, D. Benrabah, J. Y. Sanchez, *J. Power Sources* **1997**, *68*, 372–376; b) F. Alloin, J. Y. Sanchez, *J. Power Sources* **1999**, *81–82*, 795–803.
- [21] a) D. Benrabah, R. Arnaud, J. Y. Sanchez, *Electrochim. Acta* **1995**, *40*, 2437–2443; b) R. Arnaud, D. Benrabah, J. Y. Sanchez, *J. Phys. Chem.* **1996**, *100*, 10882–10891.
- [22] R. S. Porter, J. F. Johnson, *Chem. Rev.* **1966**, *66*, 1–27.
- [23] Y. Wang, A. Gozen, L. Chen, W.-H. Zhong, *Adv. Energy Mater.* **2017**, *7*, 1601767.
- [24] M. Vittadello, D. I. Waxman, P. J. Sideris, Z. Gan, K. Vezzù, E. Negro, A. Safari, S. G. Greenbaum, V. Di Noto, *Electrochim. Acta* **2011**, *57*, 112–122.
- [25] M. Piccolo, G. A. Giffin, K. Vezzù, F. Bertasi, P. Alotto, M. Guarnieri, V. Dinoto, *ChemSusChem* **2013**, *6*, 2157–2160.
- [26] V. Di Noto, N. Boaretto, E. Negro, P. E. Stallworth, S. Lavina, G. A. Giffin, S. G. Greenbaum, *Int. J. Hydrogen Energy* **2012**, *37*, 6215–6227.
- [27] C. S. Martinez-Cisneros, B. Levenfeld, A. Varez, J. Y. Sanchez, *Electrochim. Acta* **2016**, *192*, 456–466.

Manuscript received: April 9, 2021

Revised manuscript received: June 4, 2021

Accepted manuscript online: June 13, 2021